

EXO-PLANETARY TRANSITS OF LIMB BRIGHTENED LINES; TENTATIVE SI IV ABSORPTION BY HD209458B

E. SCHLAWIN¹, E. AGOL², L. M. WALKOWICZ³, K. COVEY^{1,4,5}, AND J. P. LLOYD¹

Draft version September 7, 2018

ABSTRACT

Transit light curves for stellar continua have only one minimum and a “U” shape. By contrast, transit curves for optically thin chromospheric emission lines can have a “W” shape because of stellar limb-brightening. We calculate light curves for an optically thin shell of emission and fit these models to time-resolved observations of Si IV absorption by the planet HD209458b. We find that the best fit Si IV absorption model has $R_{p,\text{Si IV}}/R_* = 0.34^{+0.07}_{-0.12}$, similar to the Roche lobe of the planet. While the large radius is only at the limit of statistical significance, we develop formulae applicable to transits of all optically thin chromospheric emission lines.

Subject headings: planets and satellites: atmospheres — stars: chromospheres — ultraviolet: planetary systems

1. INTRODUCTION

Since the first observation of a transiting exoplanet (Charbonneau et al. 2000; Henry et al. 2000), knowledge of exoplanetary radii, composition and atmospheres has grown explosively. In-transit and out-of-transit spectroscopy and photometry have revealed water absorption in HD 189733b (Beaulieu et al. 2008), atmospheric emission in TrES-1 (Charbonneau et al. 2005), a surprising number of anomalously large planets (Baraffe et al. 2010), and constraints on exoplanetary composition (Rogers & Seager 2010). Accurate transit timing can also indicate the presence of additional bodies in the system through perturbations to the transiting planet’s orbit (Agol et al. 2005; Holman & Murray 2005).

When transits are observed in stellar Lyman- α , C II, Si III, Mg II and O I emission, they show much deeper minima than for visible wavelengths, revealing escaping atmospheres extending far beyond the geometric radii⁶ of planets (Vidal-Madjar et al. 2004; Ben-Jaffel 2007; Murray-Clay et al. 2009; Lecavelier des Etangs et al. 2010; Fossati et al. 2010). These light curves also constrain atmospheric conditions and mass escape from the planet’s Roche lobe (Knutson et al. 2007; García Muñoz 2007; Linsky et al. 2010).

Transit searches have been largely in the optical and near-infrared continuum, where the star is optically thick and limb darkened due to the temperature profile at the $\tau \approx 1$ surface of the star. For limb darkened wavelengths, the flux from the transiting system is at a minimum when the planet crosses the sub-earth longitude of the star (phase = 0.0) because the stellar disk is brightest at its center.

By contrast, emission lines from stellar chromospheres and transition regions can be limb *brightened*. For optically thick emission, limb brightening occurs when the source function increases with stellar altitude. For optically thin emission, strong limb brightening occurs because the chromospheric and transition region gas has its largest column density at the edges. Assef et al. (2009) showed that transit observations of chromospheric emission lines decrease sharply to a minimum at the first limb, increases to a local maximum mid-transit and then reverses the process as the planet exits the stellar disk. As a consequence, such a transit curve will be “W”-shaped.

Assef et al. (2009) point out that limb brightening could be useful for detecting exoplanetary transits of giant stars. Light curves of limb brightened wavelengths have deeper minima than for both limb darkened and uniform disk emission. The star emits over a smaller effective area—a ring instead of a disk—so the planet covers a larger amount of the stellar flux. This is important for transits of giant stars where broadband transit depths can be below 0.01% for Jupiter-sized planets. Also, the planet covers its host’s limb for a small fraction of the transit, allowing for feasible detection of giant star transits with ground based telescopes, which suffer from systematic photometric errors over timescales longer than one night. The exoplanets 4UMa b, HD 122430b, HD 13189b, and HIP75458 b all have transit probabilities greater than 10% and may be useful targets for future studies (Assef et al. 2009).

Assef et al. (2009) approximate the limb brightened star as a central disk of emission surrounded by a circularly symmetric ring with ~ 30 times the intensity. With this ring approximation, the maximum depth of the transit is proportional to the ratio of the planet radius to stellar radius, R_p/R_* if the emission from the central disk is negligible, instead of $(R_p/R_*)^2$, as expected for a uniform disk. This is because the planet covers $\sim 2R_p$ out of a circle of emission whose total circumference is $2\pi R_*$.

In this paper, we present a transit light curve calculation for an optically-thin and geometrically-thin shell of emission. The calculated maximum transit depth scales as $(R_p/R_*)^{3/2}$, instead of R_p/R_* . In §2 we calculate

¹ Astronomy Department, Cornell University, Ithaca NY 14853

² Astronomy Department, University of Washington, Seattle, WA 98195

³ Astronomy Department, University of California at Berkeley, Berkeley, CA 94720

⁴ Visiting Scholar, Department of Astronomy, Boston University, 725 Commonwealth Ave, Boston, MA 02215

⁵ Hubble Fellow

⁶ In this paper, we define the geometric radius as the radius derived from broadband visible wavelength transit depths.

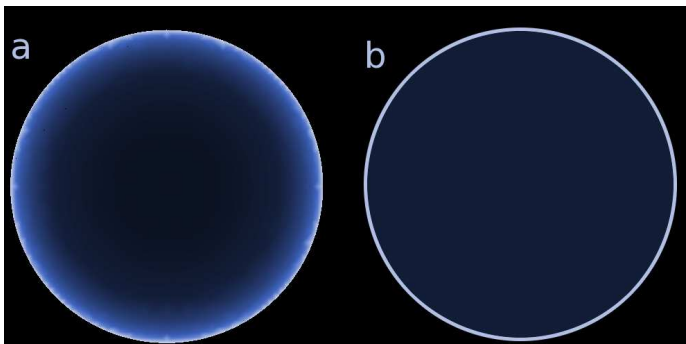


FIG. 1.— Model Limb Brightening. (a) A model of spherically symmetric optically thin emission varies continuously from limb to center. (b) An approximate model where most of the emission is from the stellar limb surrounding a uniformly emitting circle. We employ the model shown in (a) for Si IV emission, whose transit light curve is given by equation 1.

the expected limb brightened light curve for an optically thin emission line. We consider optically thin emission because it shows at least 8 times the limb brightening of optically thick emission (Kastner & Bhatia 1992). We fit this model light curve to Si IV emission from HD209458 in §3 and discuss the implications for HD209458b’s thermosphere in §4.1.

2. A LIMB BRIGHTENED CURVE UNDER THE THIN-SHELL APPROXIMATION

We make the approximation that the thickness of the chromosphere, h , is much smaller than the size of the planet (R_p) and star (R_*). Under this geometrically thin approximation, the total flux from the star is proportional to the surface area of the hemisphere facing the Earth times its thickness h , because the total flux for an optically thin emission line is proportional to the total number of emitting ions. Neglecting any photospheric contribution, the amount of emission that the planet blocks is then simply the amount of the stellar surface that the planet covers times h . In this geometrical limit, therefore, the thickness of the chromosphere, h , cancels out.

We compute the light curve for zero thickness ($h = 0$) by finding the area of the the planet’s shadow and dividing this by the surface area of a hemisphere with radius R_* . The volume of the intersection of a cylinder with a sphere is given by Lamarche & Leroy (1990) and we find the surface area of the intersection by taking a partial derivative with respect to the radius of the sphere. The result can be expressed analytically in terms of elliptic integrals. Let x be the distance, in units of stellar radii, R_* , from the center of the planet to the center of the star projected onto a plane perpendicular to the observer. Let p be the planet/star radius ratio, R_p/R_* . To calculate the light curve for a planet that does not pass through the center of the star, one can simply write $x(t)$ as $\sqrt{d^2 + b^2}$, where d is the distance to the closest approach point in stellar radii R_* and b is the impact parameter in stellar radii R_* .

The transit depth, $\delta(x)$ is a piecewise function with three different regimes: (1) when the planet is fully contained in the stellar disk (2) when the planet is at egress/ingress and (3) when the planet is beyond the stellar disk. We also include the case that the planet’s

absorption profile is larger than the star. In this case, the same formulae apply—see Equation 2. A small figure for each regime is included in the equations, where an open circle represents the star and a filled circle represents the planet.

$$\delta(x) = \Theta(p - x) + \frac{a_0}{2\pi\sqrt{xp}} \times \left[\frac{x+p}{x-p} \Pi(n, m) - 4xpa_1 E(m) - a_2 K(m) \right] \quad (1)$$

	\odot	\odot	\odot	\bullet
$p < 1$	$0 < x < 1 - p$	$1 - p < x < 1 + p$	$1 + p < x$	
$p > 1$	$p - 1 < x < 1 + p$	$0 < x < p - 1$	$\text{or } x > p + 1$	
a_0	\sqrt{m}	1	0	
a_1	$\frac{1}{m}$	1		
a_2	$x^2 - p^2$	$1 - 2p(x + p)$		
m	$\frac{4xp}{1 - (x - p)^2}$	$\frac{1 - (x - p)^2}{4xp}$		
n	$-4xp/(x - p)^2$	$1 - (x - p)^{-2}$		(2)

where $K(m)$, $E(m)$, and $\Pi(n, m)$ are the complete Legendre elliptic integrals of the first, second, and third kinds, and $\Theta(x)$ is the Heaviside step function. For the elliptic integrals, we use the conventions of Abramowitz & Stegun (1972) where $\Pi(n, m) = \Pi(n; K(m)|m)$ for the third elliptic integral.⁷

These formulae are difficult to evaluate numerically at $x = 0$, $x = p$ and $x = 1 \pm p$ due to the formal divergence of different terms in equations 1 and 2; the divergences cancel out analytically, but routines that evaluate the elliptic integrals diverge. However, these locations are a set of measure zero, and thus are tractable when modeling data.

2.1. Analytical Transit Depth Estimation

The transit is deepest slightly before second contact, so we can estimate the maximum transit depth as follows from Figure 2 by comparing the total emitting area of the star to the total stellar surface area blocked by the planet. The blocked surface is the same as the shadow produced by a sphere of radius R_p onto a hemisphere of radius R_* . When the planet occults the edge of the star (second contact), as shown from an edge-on viewpoint in this figure, then the length of the arc of the long axis of the shadow is $R_*\theta$. The diameter of the planet is $2R_p \approx R_*(1 - \cos\theta) \approx \frac{1}{2}R_*\theta^2$, where the latter approximation is valid for $\theta \ll 1$. We can approximate the shadow as an ellipse with a semi-minor axis of R_p and a semi-major axis of $\frac{1}{2}R_*\theta$, so the area of the shadow is $A_t = \pi\sqrt{R_p R_* R_p}$. Thus, the maximum depth of transit is

⁷ An IDL procedure for the transit depth $\delta(x)$ is located at <http://www.astro.washington.edu/ago1/>.

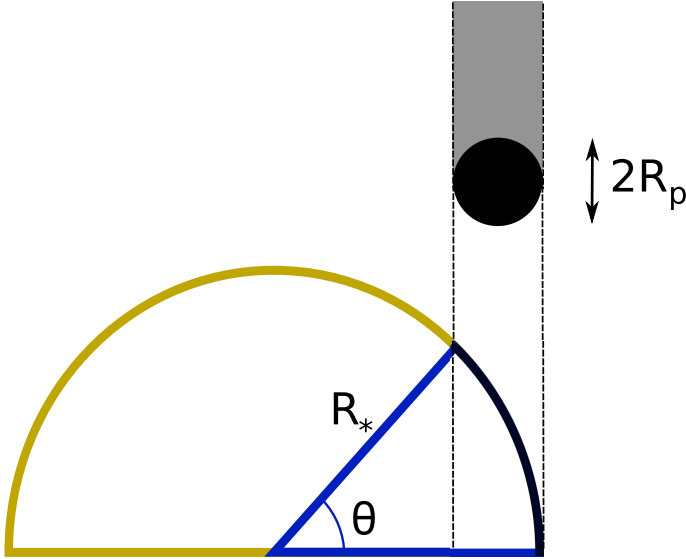


FIG. 2.— Edge-on view of area of stellar emission and the amount blocked by a planet. This blocked surface area is the same as the area of a shadow cast by a sphere onto a hemisphere.

given by

$$\delta_{\max} \approx \frac{A_t}{2\pi R_*^2} = \frac{1}{2} \left(\frac{R_p}{R_*} \right)^{3/2} \quad (3)$$

which is accurate to within 5% for $R_p/R_* < 0.23$. Note that this is a different scaling for maximum transit depth than that given in Assef et al. (2009) who assume that most of the stellar emission is from a thin ring. For $R_p/R_* = 1 - \sqrt{3}/2$, half of the stellar emission is within R_p of the stellar radius R_* , so for $R_p/R_* \gtrsim 0.13$, the ring approximation is valid, but the scaling of transit depth assumes negligible limb curvature at the scale of the planet ($R_p/R_* \ll 1$).

The remarkable consequence of Equation 3 is that the depth of a chromospheric transit does not decline as much with the radius of the planet as a transit of a uniform disk. A chromospheric transit has a maximum depth that is $\approx \frac{1}{2} \left(\frac{R_*}{R_p} \right)^{1/2}$ times deeper than the maximum transit depth of a uniform disk; thus smaller planets have an advantage to be observed at chromospheric wavelengths, as emphasized by Assef et al. (2009). It should also be noted that at mid-transit, the Double-U curve has a smaller transit depth than for a uniform disk, because the planet covers only πR_p^2 out of a hemisphere of area $2\pi R_*^2$.

Figure 3 (solid curve) shows the transit light curve, $1 - \delta(x)$, for a planet that has $R_p/R_* = 0.08$. The estimate given by equation 3 and the more detailed equation 1 agree well, predicting maximum chromospheric depths to be 1.8 times deeper than for uniform disk brightness. (For a uniform disk emission $\delta_{\max} = \pi R_p^2 / (\pi R_*^2)$). We also include a light curve for the thin circle of emission shown in Figure 1 b for comparison.

3. Si IV ABSORPTION BY HD 209458B

Vidal-Madjar et al. (2003, 2004) observed the exoplanet host HD 209458 with the Hubble Space Telescope Imaging Spectrograph (STIS) instrument and found

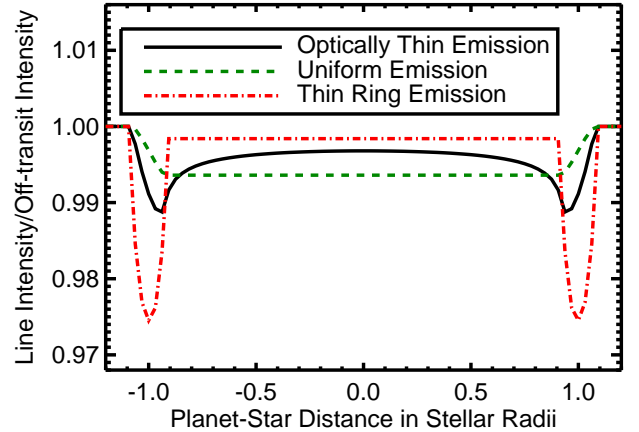


FIG. 3.— Transit light curve for $R_p/R_* = 0.08$, using a family of 3 different models. The solid line is for a transit of an optically thin shell using equation 1 where the emission looks like Figure 1 a. The “Uniform Emission” (Mandel & Agol 2002, dashed green line) is one for which the emission is assumed to be constant across the stellar disk. The “Thin Ring Emission” model (dot-dash red line) is a model where the emission is assumed to be mostly from a thin ring as pictured in Figure 1 b. Note that the “Thin Ring” and “Optically Thin Emission” models’ minima are deeper than the uniform emission model and that these minima occur near the stellar limbs.

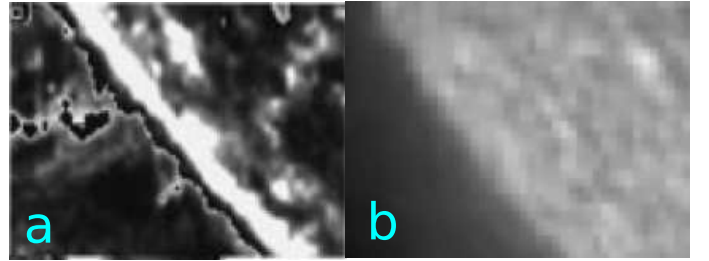


FIG. 4.— (a) Si IV emission from the Solar limb as observed by SUMER (Solar Ultraviolet Measurement of Emitted Radiation) (Wiik et al. 1997) is strongly limb-brightened, indicating that a transit of this emission line should have a Double-U light curve. (b) He II 304 Å image of the solar limb, taken by the Extreme-ultraviolet Imaging Telescope (Feldman et al. 2000) is, by contrast, not limb brightened because it is optically thick in the chromosphere and thus the additional column density at the limb does not contribute any more flux than the central disk.

an extended hydrogen, oxygen and carbon atmosphere around the planet by fitting the light curves to the H I, O I and C II lines during a transit. Vidal-Madjar et al. (2004) found no Si IV absorption when fitting the light curve to a model of a spherical planet occulting a *uniform* stellar disk.

We fit their Si IV 1394 Å data (Vidal-Madjar et al. (2004), Figure 3) with a Double-U model given by equation 1. This model is appropriate for the Si IV emission, as evident in the Solar image in Figure 4 (a) where strong limb-brightening is apparent. France et al. (2010) found that the Si IV 1394 Å / Si IV 1403 Å ratio is 2:1 within the errors, indicating that the Si IV 1394 Å emission is optically thin (Bloomfield et al. 2002; Christian et al. 2006). We investigated the transit of the Si IV line because it the strongest optically thin line in HD209458b’s STIS

spectrum. While other limb brightened emission lines do exist, we focus on the optically thin ones because they should be the most limb brightened.

The model has two free parameters: the planet/star radius ratio R_p/R_* and an overall constant that sets the off-transit flux. The second parameter is necessary since the off-transit Si IV 1394 Å STIS flux is poorly constrained. The impact parameter is fixed with a value of $b = 0.50R_*$, using an inclination of 86.7° and a semi-major axis $a = 8.76R_*$ (Torres et al. 2008).

Figure 5 shows the light curve for the Vidal-Madjar et al. (2004) data and the best fit model. In addition to the best fit model, we show two more limb brightened models where R_p/R_* is a fixed parameter for comparison. These have R_p/R_* equal to 0 and 0.12, representing no Si IV absorption and the geometric planet radius (Knutson et al. 2007), respectively.

Using a Levenberg-Marquardt fitting algorithm (Markwardt 2009) and the points at which the $\chi^2 - \chi^2_{min} = 1$ to calculate uncertainties, we find that $R_p/R_* = 0.34^{+0.07}_{-0.12}$, close to the size of the Roche Lobe. The Double-U model has a total χ^2 of 10.4 with 12 data points and two parameters, which is 3.1 less than fitting the data to a constant flux line (representing no detection) with one parameter. Since these models are nested, we can use the maximum likelihood ratio test. The P-value for the difference in χ^2 is 0.05, so the data favor the Double-U model with 95% confidence, assuming normally distributed data. The same test favors the $R_p/R_* = 0.34$ model over the $R_p/R_* = 0.12$ model with 91% confidence.

4. CONCLUSION

As indicated by the Solar image of Si IV in Figure 4, a limb brightened model should be used for Si IV emission. The Double-U model for the Si IV transit fits the data better than a non-detection, even when accounting for the additional parameters in the model. The best fit absorption radius $R_p/R_* = 0.34^{+0.07}_{-0.12}$, if the absorption is entirely optically thick. This radius favors planetary atmosphere models with mass flow beyond the planet’s Roche lobe.

The best time to observe transits in optically thin stellar emission lines is when a planet crosses its host’s limb and not at a phase of 0, since the Double-U curve is deepest at the stellar limb. Observations at the limb have a depth of $\sim 0.5 (R_p/R_*)^{3/2}$ whereas at the center of the star they have a transit depth of $\sim 0.5 (R_p/R_*)^2$, only half the depth of a uniform brightness transit.

4.1. Discussion

The Si IV transit depth is comparable to the O I transit depth calculated by Vidal-Madjar et al. (2004) and larger than the H I transit depth calculated by Ben-Jaffel (2007). As Koskinen et al. (2010) point out, a hard sphere, which we assume in equation 1, is a poor approximation to planetary atmospheric absorption. The Si IV absorption profile, instead of having a sharp transition from opaque to transparent, should change smoothly from optically thick to optically thin absorption in a more accurate model. In order to explain the large transit depth, this smooth model would have to have a radius

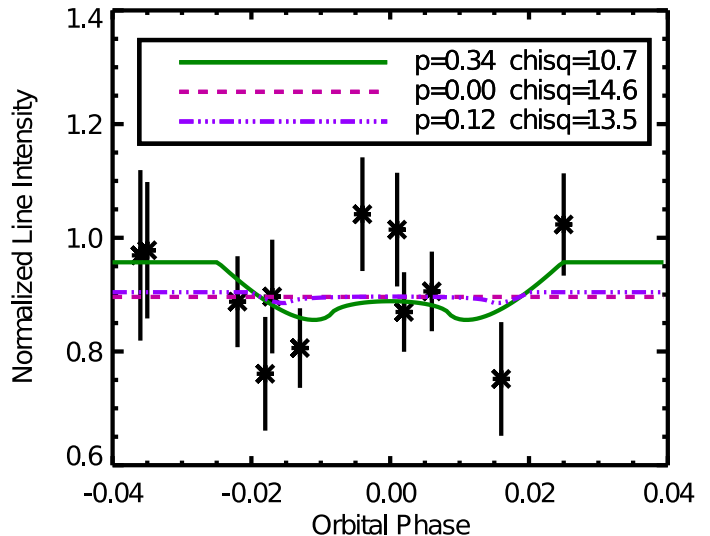


FIG. 5.— The light curve of the limb-brightened transition region line Si IV during the transit of HD209458b, as taken by Vidal-Madjar et al. (2004) for a wavelength range of [1391 Å, 1397 Å]. Fluxes are normalized so that the weighted average of the points when the planet is not occulting the star is 1.0. The solid line is a best fit model, using equation 1 where the radius is a free parameter. For reference, two different best-fit models are shown where the planet size is a fixed parameter: the dashed curve is a horizontal line, corresponding to $R_p/R_* = 0$ or a non-detection of Si IV absorption. The dash triple-dotted line is a model with the geometric radius, $R_p/R_* = 0.12$. The best-fit radius, $R_p/R_* = 0.34$ (normalized $\chi^2 = 1.07$), indicates Si IV absorption from a Roche lobe-sized cloud.

extending beyond the planet’s Roche lobe to explain the observed transit depth. R_{Roche}/R_* varies from 0.35 to 0.48 (Ben-Jaffel & Sona Hosseini 2010).

The best-fit transit depth supports models with high concentrations of metallic ions in the atmosphere because the radius of Si IV absorption is as large as for H I absorption. Koskinen et al. (2010) point out that if the metallicity is high, the temperature must also be elevated. The $\sim 10,000$ K temperature suggested by García Muñoz (2007), Murray-Clay et al. (2009), and Koskinen et al. (2010) for the thermosphere may not explain the large abundances of Si^{3+} needed for the observed absorption. The ionization energy, $\Delta E/k$ for $\text{Si}^{2+} \rightarrow \text{Si}^{3+} = 3.9 \times 10^5 \text{K}$, suggests that the Si^{3+} may be produced in a shock between the stellar and planetary winds.

Linsky et al. (2010) find no significant Si IV absorption by HD209458b. Our best fit to the STIS data predicts the average transit depth to be $9^{+4}_{-5}\%$ for the same phases as their observations, but Linsky et al. (2010), with the Cosmic Origins Spectrograph (COS), found $0.2 \pm 1.4\%$. These results disagree at the $\sim 1.7\sigma$ level and variability in the planet’s atmosphere may account for the discrepancy. Linsky et al. (2010) did observe some weak Si IV absorption features found at +20 and +40 km/s in their spectrum, which indicates that some Si^{3+} ions remain in the planet’s atmosphere or winds.

Linsky et al. (2010) suggest that the amount of another Silicon ion, Si^{2+} , may vary appreciably over short timescales because of changes in stellar wind speed, planetary mass-loss rate or temperature fluctuations. Conversely to Si IV, for which 2003 STIS observations indicate strong absorption and 2009 COS observations

indicate weak absorption, the Si III absorption is seen strongly in absorption in the 2009 COS data and weakly in the 2003 STIS data.

Additional observations will help confirm or refute the detection of Si³⁺ in the thermosphere of HD209458b. The Cosmic Origins Spectrograph (COS) is an ideal instrument with 2 to 10 times the sensitivity of previous ultraviolet spectrographs (Froning & Green 2009). COS was used by Linsky et al. (2010), but only when HD209458b was close to a phase of 0.0, 0.25, 0.5 and 0.75 and once when the planet was at the stellar limb. Additional observation at the host's limb would be optimal for Si IV and other optically thin emission lines. With enough signal to noise, the light curve may reveal asymmetries in the transit having to do with an asymmetric spatial distribution of the UV-absorbing cloud. The advantage of the limb brightened emission lines is that they come from a smaller spatial area of the star

and therefore probe the spatial distribution of the planetary atmosphere better than optically thick emission. Accurate time resolved transit data may also reveal differences in *thermal* properties of the leading and trailing sides of the planet as predicted by Fortney et al. (2010).

E. Schlawin was supported by the NASA Space Grant Fellowship. E. Agol was supported in part by the NSF under Grant No. PHY05-51164 during a visit to the Kavli Institute for Theoretical Physics, and by NSF CAREER Grant No. 0645416. Support for Kevin Covey was provided by NASA through Hubble Fellowship grant #HST-HF-51253.01-A awarded by the Space Telescope Science Institute, which is operated by the Association of Universities for Research in Astronomy, Inc., for NASA, under contract NAS 5-26555. Lucianne Walkowicz is grateful for the support of the Kepler Fellowship for the Study of Planet-Bearing Stars.

REFERENCES

- Abramowitz, M. & Stegun, I. A. 1972, Handbook of Mathematical Functions, ed. Abramowitz, M. & Stegun, I. A.
- Agol, E., Steffen, J., Sari, R., & Clarkson, W. 2005, MNRAS, 359, 567
- Assef, R. J., Gaudi, B. S., & Stanek, K. Z. 2009, ApJ, 701, 1616
- Baraffe, I., Chabrier, G., & Barman, T. 2010, Reports on Progress in Physics, 73, 016901
- Beaulieu, J. P., Carey, S., Ribas, I., & Tinetti, G. 2008, ApJ, 677, 1343
- Ben-Jaffel, L. 2007, ApJ, 671, L61
- Ben-Jaffel, L. & Sona Hosseini, S. 2010, ApJ, 709, 1284
- Bloomfield, D. S., Mathioudakis, M., Christian, D. J., Keenan, F. P., & Linsky, J. L. 2002, A&A, 390, 219
- Charbonneau, D., Allen, L. E., Megeath, S. T., Torres, G., Alonso, R., Brown, T. M., Gilliland, R. L., Latham, D. W., Mandushev, G., O'Donovan, F. T., & Sozzetti, A. 2005, ApJ, 626, 523
- Charbonneau, D., Brown, T. M., Latham, D. W., & Mayor, M. 2000, ApJ, 529, L45
- Christian, D. J., Mathioudakis, M., Bloomfield, D. S., Dupuis, J., Keenan, F. P., Pollacco, D. L., & Malina, R. F. 2006, A&A, 454, 889
- Feldman, U., Dammasch, I. E., & Wilhelm, K. 2000, Space Science Reviews, 93, 411
- Fortney, J. J., Shabram, M., Showman, A. P., Lian, Y., Freedman, R. S., Marley, M. S., & Lewis, N. K. 2010, ApJ, 709, 1396
- Fossati, L., Haswell, C. A., Froning, C. S., Hebb, L., Holmes, S., Kolb, U., Helling, C., Carter, A., Wheatley, P., Cameron, A. C., Loeillet, B., Pollacco, D., Street, R., Stempels, H. C., Simpson, E., Udry, S., Joshi, Y. C., West, R. G., Skillen, I., & Wilson, D. 2010, ApJ, 714, L222
- France, K., Stocke, J. T., Yang, H., Linsky, J. L., Wolven, B. C., Froning, C. S., Green, J. C., & Osterman, S. N. 2010, ApJ, 712, 1277
- Froning, C. S. & Green, J. C. 2009, Ap&SS, 320, 181
- García Muñoz, A. 2007, Planet. Space Sci., 55, 1426
- Henry, G. W., Marcy, G. W., Butler, R. P., & Vogt, S. S. 2000, ApJ, 529, L41
- Holman, M. J. & Murray, N. W. 2005, Science, 307, 1288
- Kastner, S. O. & Bhatia, A. K. 1992, ApJ, 401, 416
- Knutson, H. A., Charbonneau, D., Noyes, R. W., Brown, T. M., & Gilliland, R. L. 2007, ApJ, 655, 564
- Koskinen, T. T., Yelle, R. V., Lavvas, P., & Lewis, N. K. 2010, ArXiv e-prints
- Lamarche, F. & Leroy, C. 1990, Computer Physics Communications, 59, 359
- Lecavelier des Etangs, A., Ehrenreich, D., Vidal-Madjar, A., Ballester, G. E., Desert, J., Ferlet, R., Hébrard, G., Sing, D. K., Tchakoumegni, K., & Udry, S. 2010, ArXiv e-prints
- Linsky, J. L., Yang, H., France, K., Froning, C. S., Green, J. C., Stocke, J. T., & Osterman, S. N. 2010, ArXiv e-prints
- Mandel, K. & Agol, E. 2002, ApJ, 580, L171
- Markwardt, C. B. 2009, in Astronomical Society of the Pacific Conference Series, Vol. 411, Astronomical Society of the Pacific Conference Series, ed. D. A. Bohlender, D. Durand, & P. Dowler, 251–+
- Murray-Clay, R. A., Chiang, E. I., & Murray, N. 2009, ApJ, 693, 23
- Rogers, L. A. & Seager, S. 2010, ApJ, 712, 974
- Torres, G., Winn, J. N., & Holman, M. J. 2008, ApJ, 677, 1324
- Vidal-Madjar, A., Désert, J., Lecavelier des Etangs, A., Hébrard, G., Ballester, G. E., Ehrenreich, D., Ferlet, R., McConnell, J. C., Mayor, M., & Parkinson, C. D. 2004, ApJ, 604, L69
- Vidal-Madjar, A., Lecavelier des Etangs, A., Désert, J., Ballester, G. E., Ferlet, R., Hébrard, G., & Mayor, M. 2003, Nature, 422, 143
- Wiik, J. E., Schmieder, B., Kucera, T., Poland, A., Brekke, P., & Simnett, G. 1997, Sol. Phys., 175, 411